Water Supply

IWA PUBLISHING

Water Supply Vol 22 No 4, 3814 doi: 10.2166/ws.2022.023

Further investigation of the irreversible floc breakup in flocculation kinetics modelling

Rodrigo de Oliveira Marques [a,b,*] and Sidney Seckler Ferreira Filho [a,b]

[a] Hydraulic and Environmental Engineering Department, Polytechnic School, University of Sao Paulo, Sao Paulo, Brazil
[b] Departamento de Engenharia Hidráulica e Ambiental, Escola Politécnica, Universidade de São Paulo, Avenida Professor Almeida Prado, número 83, Travessa 2 – Cidade Universitária, São Paulo, SP CEP: 05508 900, Brasil
*Corresponding author. E-mail: rodrigo.oliveira.marques@usp.br

R de OM, 0000-0002-9285-055X; SSFF, 0000-0002-5153-4665

ABSTRACT

Recent research has shown that the equilibrium between aggregation and breakup in flocculation kinetics modelling may not hold due to irreversible floc breakup. This work investigated the influence of the coagulant/particle ratio and average velocity gradient ($\bar{G}$) in the occurrence of this phenomenon with a different water matrix than previous research. Jar test assays were conducted with low (≈15 NTU), medium (≈50 NTU) and high (≈100 NTU) turbidity synthetic raw water, using alum as coagulant and kaolin as primary particles. Results were analyzed using Argaman and Kaufman's model and values for K_A (aggregation constant) and K_B (breakup coefficient) were determined with the evolutionary convergence method. Model fitting was satisfactory when the Al/particle ratio varied between 10 and 27 mg Al^{3+}/g. Outside this range, residual turbidity increased after equilibrium, attributed to the irreversible floc breakup process and not adequately described by the model. A two-factor analysis of variance (ANOVA) was conducted, and the results indicated a plausible correlation between pK_A (–log K_A) and Al/particle ratio. As for pK_B (–log K_B), the results indicated a possible correlation with both Al/particle ratio and $\bar{G}$. The results suggest that the irreversible floc breakup may occur regardless of the water matrix composition.

Key words: average velocity gradient, floc breakup, flocculation, kinetics, modelling, water treatment

HIGHLIGHTS

- Equilibrium between aggregation and breakup processes in Argaman and Kaufman's original model may not hold.
- Residual turbidity increase was observed and attributed to the irreversible floc breakup process.
- This phenomenon was not adequately captured by Argaman and Kaufman's original model.
- Coagulant/particle ratio may play a critical role.
- The irreversible floc breakup may occur regardless of the water matrix.

INTRODUCTION

The flocculation process is essential to water treatment, especially when solid and liquid phases are separated via sedimentation. In this perspective, flocculation units in conventional drinking water treatment plants (DWTPs) should minimize floc breakup due to its negative impact on solid separation efficiency (AWWA 2011; Crittenden *et al.* 2012; Bratby 2016).

In the last few years, process modelling has become a powerful tool for design and operation. However, due to its complexity, flocculation still requires a universal model (Thomas *et al.* 1999; Watanabe 2017). Argaman and Kaufman's original model, although knowingly limited for design purposes, can be useful for the evaluation of existing units and routine process control since it requires only results from jar test assays (Argaman & Kaufman 1970; Bratby 2016). This is particularly interesting for DWTPs in developing countries, as they usually are not equipped with sophisticated laboratories (Di Bernardo *et al.* 2017; Ferreira Filho 2017).

Argaman and Kaufman developed their mechanistic model in 1970 and it was a breakthrough at the time since it comprised both aggregation and breakup processes in its formulation. As depicted by the authors, both processes occur simultaneously, and an equilibrium is eventually reached if the initial conditions are kept constant. Equation (1) presents

the classic working equation for this model (AWWA 2011; Crittenden *et al.* 2012; Bratby 2016):

$$\frac{dN}{dt} = -K_A.N.\bar{G} + K_B.N_0.\bar{G}^2 \quad (1)$$

where dN/dt is the rate of change in the concentration of primary particles ($ML^{-3}T^{-1}$); $\bar{G}$ is the average velocity gradient (T^{-1}); N is the primary particles concentration at a specific time (ML^{-3}); N_0 is the initial primary particle concentration (ML^{-3}); K_A is the aggregation constant (–) and K_B is the breakup coefficient (T).

Analytical integration of the working equation for a batch reactor allows to model particle concentration (N_t) at a specific time, given the values for $\bar{G}$, N_0, K_A, K_B (Levenspiel 1999; Bratby 2016). Residual turbidity data from jar test assays can be used as a surrogate for particle concentration (Tassinari *et al.* 2015). Although usually referred as constants, K_A (Equation (2)) and K_B (Equation (3)) are, in fact, coefficients and its values should be determined experimentally for each system (Bratby 2016):

$$K_A = K_F.K_S.K_P \quad (2)$$

$$K_B = \frac{3}{4.\pi}\frac{B.\phi.K_p^2}{N_0.R_1^2K_2} \quad (3)$$

K_A depends on the value of the flocculation constant K_F, equivalent to $3.\alpha.\phi$ (where α is the collision efficiency factor and ϕ is the floc volume fraction); K_S, a proportionality coefficient, indicates the effect of the turbulence energy spectrum on the effective diffusion coefficient; and K_P is the stirrer performance coefficient ($L^2.T^{-1}$). K_A is affected by the chemical composition (K_F) and, at some level, by the mixing aspects of the system (K_S and K_P). In coagulation-pH fixed systems, the volume fraction, ϕ, depends on the coagulant dosage. On the other hand, the formula for K_B depends on a generic breakup constant B (–); R_1, which is the radius of the primary particle (L), and K_2, a constant that relates the average floc size with the mean square fluctuating velocities. Two aspects stand out in Equation (3). First, the K_B value is directly proportional to the value of Φ, suggesting that excessive dosages may increase the occurrence of the rupture process. Second, K_B is also directly proportional to the value of K_P squared, indicating that K_B is more influenced by the mixing aspects of the system than K_A (Argaman & Kaufman 1970; Haarhoff & Joubert 1997; Crittenden *et al.* 2012; Bratby 2016; Di Bernardo *et al.* 2017; Ferreira Filho 2017).

Despite its limitations, Argaman and Kaufman's model still holds potential for application and can provide useful information. Although the model was developed in the early 1970s, just a handful of publications report calculated values for K_A and K_B and an extensive database is not available (Haarhoff & Joubert 1997; Ferreira Filho *et al.* 2000; Di Bernardo *et al.* 2005; Crittenden *et al.* 2012; Moruzzi & de Oliveira 2013; Bratby 2016; Marques & Ferreira Filho 2017). Providing data for these coefficients is critical, especially when correlated with raw water composition and coagulant/particle ratio, as it can be useful for future studies and predictive model applications. Moreover, previous methods for determining K_A and K_B values were mostly manual computations (Argaman & Kaufman 1970; Bratby 1981; Haarhoff & Joubert 1997). Today, the increase of technology has brought new computational methods that can be used to calculate these coefficients. An example is the use of genetic algorithms to approach a global minimum value (Brandt 2014; Winston 2016). Lastly, Argaman and Kaufman's model was developed assuming that a permanent equilibrium between aggregation and breakup is achieved if initial conditions do not change. Recent research has shown that this equilibrium may not hold, even if initial conditions are constant, possibly giving rise to an irreversible floc breakup phenomenon (Jarvis *et al.* 2004, 2005a, 2005b; Marques & Ferreira Filho 2017).

Therefore, this paper aimed to investigate Argaman and Kaufman's original model seeking to identify trends in experimental results that could be related to the irreversible floc breakup phenomenon. Values for K_A and K_B were determined for each assay using a novel numerical approach providing additional data for future research. Main variables, such as coagulant/particle ratio and $\bar{G}$ were statistically evaluated to provide new insights to model applicability.

METHODS

Synthetic raw water stock preparation

To simulate variations of raw waters' turbidity, 200 L stocks of water from the public supply system were spiked with 6.5, 24, and 48 g of kaolin, resulting in initial turbidities values of 15 (low), 50 (medium) and 100 NTU (high), respectively. A sample was collected for physical-chemical characterization from each stock prepared (Rice *et al.* 2012). Results are presented in the Supplementary Material section.

Flocculation kinetics assays

Flocculation kinetics assays were grouped in terms of initial turbidity of the raw water stock (low, medium, and high). Within each group, 36 assays were conducted, each combining one of six aluminum sulfate $Al_2(SO_4)_3{\cdot}18H_2O$ dosages and one of six $\bar{G}$ values for flocculation. Low turbidity group doses were 10, 20, 30, 40, 60, and 80 mg·L^{-1} (expressed as mass of the chemical product). For the other groups (medium and high turbidity), the lower 10 mg·L^{-1} dose was replaced with a higher dosage of 100 mg·L^{-1}. For all the assays, $\bar{G}$ values were 20, 30, 40, 60, 80 and 100 s^{-1}. For each coagulant dosage, a titration curve was prepared to determine the required volume of NaOH and HCl 0,1 N solutions. Coagulation pH was kept between 6.0 and 6.5 to maximize the sweep mechanism.

All the assays were conducted in a standard Nova Ética jar test device with 12 2-liter jars. Rapid mixing was kept for 30 seconds on a 236 rpm rotation (device's maximum), corresponding to a $\bar{G}$ value of approximately 600 s^{-1} and a Camp Number of 18.000 (AWWA 2011; Crittenden *et al.* 2012). Alum and base (or acid) were added simultaneously in each of the 12 jars prior to the start of the rapid mixing stage. After coagulation, rotation was reduced to match the desired $\bar{G}$ for flocculation. Twelve flocculation times were selected: 2.5, 5.0, 7.5, 10.0, 12.5, 15.0, 20.0, 25.0, 30.0, 40.0, 50.0 and 60.0 minutes, each one assigned to a specific jar. Once the flocculation time was reached, stirring was stopped to initiate the sedimentation process. After the non-ideal settling time (i.e. time during which the fluid inside the jars remained under agitation after the stirring stopped), the real settling time was recorded. For this experiment, 4 minutes was selected, resulting in a settling velocity (v_s) of 2 cm.min^{-1}, a typical value within the usual design criteria for conventional clarifiers in DWTPs (AWWA 2011; Crittenden *et al.* 2012; Ferreira Filho 2017). After settling, a sample was collected from each jar for residual turbidity (N_t) analysis. Turbidity analyses were performed using a bench scale turbidimeter (2100N from Hach). This equipment provided a $\pm$ 2% level of precision for analyses between 0 and 1000 NTU, an appropriate range for the expected experimental values. Preliminary tests indicated that turbidity results did not vary significantly if more than one measurement was taken from the same sample. Therefore, the first turbidity recorded value for each sample was used for model fitting. Turbidity was used as a surrogate parameter for particle concentration due to its analytical simplicity (Rice *et al.* 2012).

Model fitting and K_A and K_B calculation

Model fitting and K_A and K_B calculation were accomplished via the Least Squares Method. Electronic spreadsheets were prepared in Microsoft Excel 2016® software and the sum of the squares of the residuals (SSR) between modeled and experimental N_t/N_0 data was minimized with Solver function. For this work, the evolutionary convergence method was selected since it is based on genetic algorithms and more likely to find the global minimum. The evolutionary convergence method was set with a convergence criteria of 10^{-6}; mutation rate of 0.5; population size of 100; one random seed and 30 seconds as the maximum time without improvement. K_A and K_B values were set to a positive value. Model goodness-of-fit was verified with the Coefficient of Determination (CoD). A two-way factor variance analysis (ANOVA) was conducted with K_A and K_B values (converted to pK_A and pK_B) using Microsoft Excel 2016® embedded data analysis tools. A significance level of 5% ($p < 0.05$) was selected and both Al/particle ratio (mg Al^{3+}/g kaolin particle) and $\bar{G}$ values were selected as factors (Dobre & Sanchez Marcano 2007; Brandt 2014; Chapra & Canale 2015; Winston 2016; Von Sperling *et al.* 2020).

RESULTS AND DISCUSSION

Low turbidity raw water assays

Figure 1 (left) presents model fitted curves to experimental data of assays with low-turbidity raw water (≈15 NTU), 10 mg·L^{-1} of alum and $\bar{G}$ values of 20 and 30 s^{-1}. The equilibrium predicted by Argaman and Kaufman's model was not achieved, although both curves seem to approach stabilization. This data indicates a prevalence of the aggregation process with minimal influence of the breakup process (supported by the practically null values of K_B). CoD values of 0.96 and 0.97 (for $\bar{G}$ values of 20 and 30 s^{-1}, respectively) indicate that, although the equilibrium was not fully achieved, the model was able to

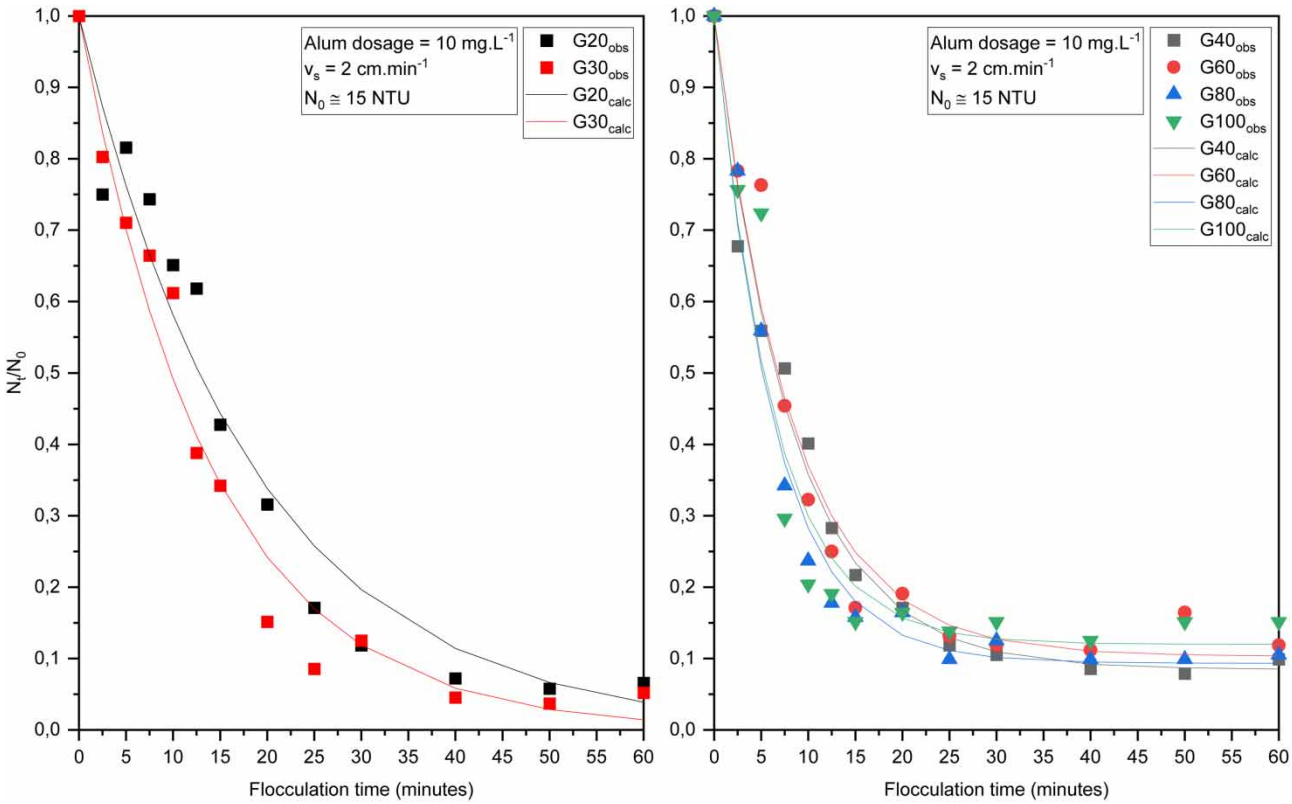

Figure 1 | Left: Model fitting to N_t/N_0 results with $\bar{G}$ values of 20 and 30 s^{-1}. Right: Model fitting to N_t/N_0 results with $\bar{G}$ values of 40, 60, 80, and 100 s^{-1}. All results with low-turbidity raw water (≈15 NTU), 10 mg·L^{-1} of alum and 2.0 cm.min^{-1} of settling velocity.

reasonably represent the experimental results. Increasing $\bar{G}$ value with the same dosage led to the equilibrium, as depicted on the right of Figure 1. With 40, 60, 80, and 100 s^{-1} the equilibrium between aggregation and breakup was achieved with approximately 30 minutes of flocculation time. Model fitting was satisfactory since CoD values were high (above 0.9 for all $\bar{G}$ values). All K_A and K_B values, minimum N_t/N_0, and CoD results are presented in the Supplementary Material for all assays.

With an alum dosage of 20 mg·L^{-1}, equilibrium was achieved with $\bar{G}$ values of 20 and 30 s^{-1}, as depicted in Figure 2. Increasing coagulant dosage usually increases K_A value (Argaman & Kaufman 1970; Bratby 2016) and since K_B values remained considerably low, equilibrium was achieved in a low N_t/N_0 level (0.10 and 0.20) with approximately 30–35 minutes. Higher $\bar{G}$ values led to equilibrium faster, however at a higher N_t/N_0 value (worsen clarified water quality). Considering Argaman and Kaufman's equations, these results are reasonable since the breakup term is related to $\bar{G}$ squared. Higher N_t/N_0 values could reduce downstream filter performance in a conventional DWTP (AWWA 2011; Crittenden *et al.* 2012).

However, a key aspect in Figure 2 is the experimental N_t/N_0 increase after equilibrium, particularly notable when $\bar{G}$ is 60, 80, and 100 s^{-1}. Model curves do not follow this trend, remaining fixed at the theoretical equilibrium, thus reducing CoD values with higher $\bar{G}$ (0.94, 0.97, 0.95, 0.88, 0.82 and 0.85 for 20, 30, 40, 60, 80 and 100 s^{-1}, respectively). Argaman and Kaufman's model was developed considering floc breakup through shear effect. However, it is known today that there are other acting mechanisms, such as an irreversible floc breakup, attributed to the residual turbidity increase trend observed (Jarvis *et al.* 2004, 2005a, 2005b; Marques & Ferreira Filho 2017).

Higher alum dosages (30, 40, 60, and 80 mg·L^{-1}) seemed to intensify this trend, as it became notable even in lower $\bar{G}$ values, suggesting that coagulant dosage plays a critical role. It is hypothesized that in excessive dosages, metal hydroxides are fragile and may break up in an irreversible way (Jarvis *et al.* 2005a; Marques & Ferreira Filho 2017), not captured by Argaman and Kaufman's original model. Thus, coagulant dosage was analyzed in terms of Al/particle ratio (mg Al^{3+}/g kaolin particle) to support this hypothesis. When alum dosage was 80 mg·L^{-1}, the Al/particle ratio was 199 mg Al^{+3}/g and resulted in residual turbidity increase already with $\bar{G}$ equal to 20 s^{-1}. In Figures 1 and 2, this ratio was roughly 25 and 50 mg Al^{3+}/g,

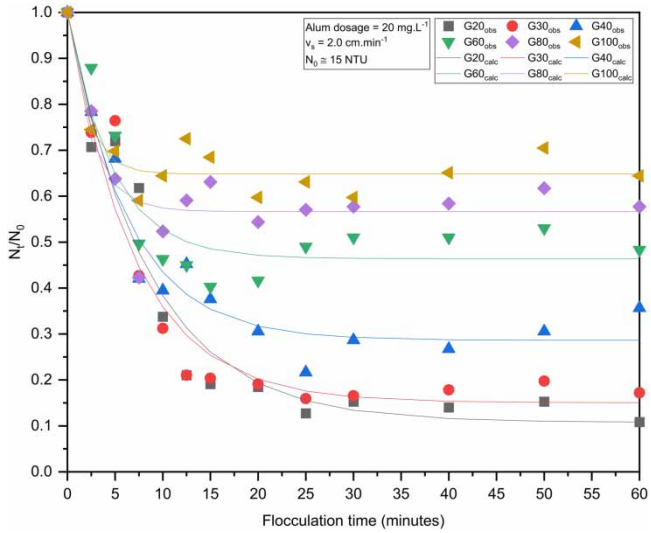

Figure 2 | Model fitting to N_t/N_0 results with low-turbidity raw water (≈15 NTU), 20 mg·L^{-1} of alum, all $\bar{G}$ values and 2.0 cm.min^{-1} of settling velocity.

respectively. However, only in Figure 1 was the residual turbidity increase not significantly observed. Therefore, 25 mg Al^{+3}/g was considered an optimal ratio for the low-turbidity raw water.

Medium turbidity raw water assays

In Figure 3 all $\bar{G}$ values led to the equilibrium predicted in Argaman and Kaufman's model. It is notable that for $\bar{G}$ values of 20, 30, and 40 s^{-1}, the process reached equilibrium later than for the remaining $\bar{G}$ values. However, increasing mixing intensity did not result in significant increase in the N_t/N_0 ratio, thus indicating that the 20 mg·L^{-1} alum dosage (14 mg Al^{3+}/g ratio) did not lead to the residual turbidity increase trend (attributed to the irreversible floc breakup). With alum dosages of 30 and 40 mg·L^{-1}, the same behavior was observed (20 and 27 mg Al^{3+}/g ratios, respectively). CoD values for all these ratios were higher than 0.9, indicating reasonable model fitting.

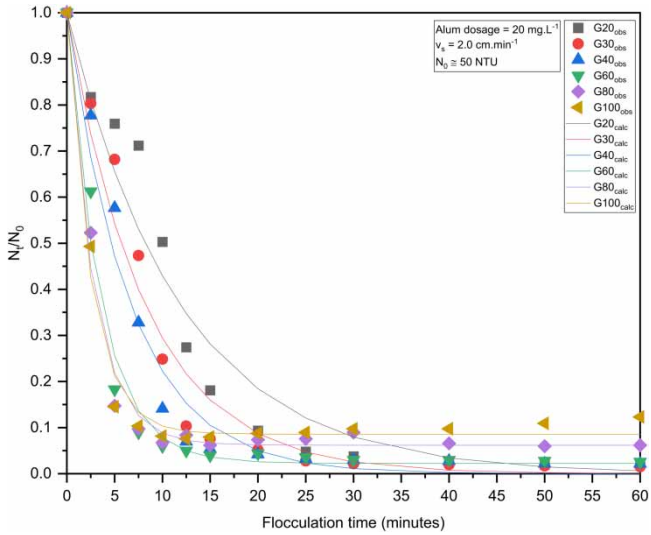

Figure 3 | Model fitting to N_t/N_0 results with low-turbidity raw water (≈50 NTU), 20 mg·L^{-1} of alum, all $\bar{G}$ values and 2.0 cm.min^{-1} of settling velocity.

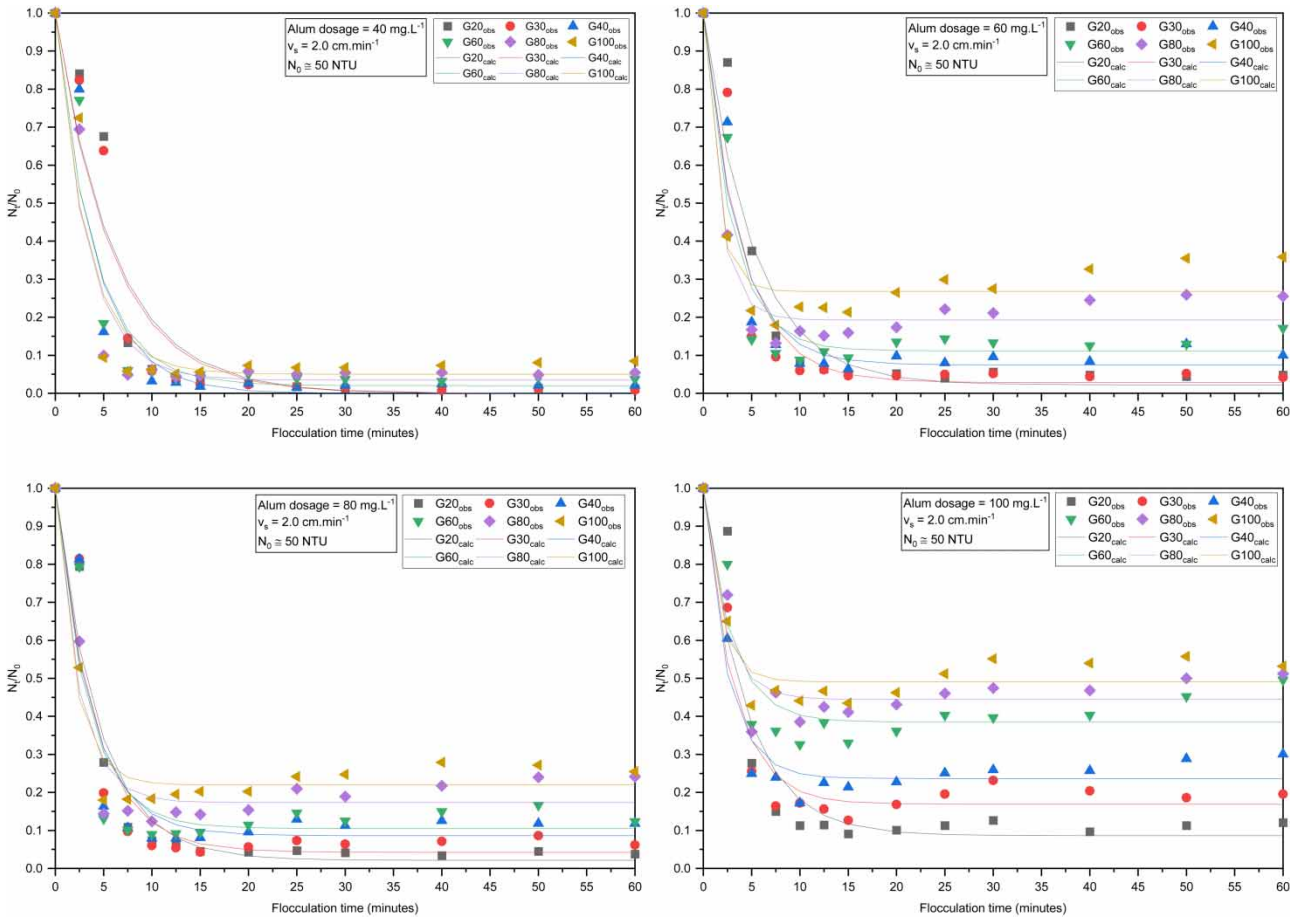

Figure 4 | Model fitting to N_t/N_0 results with medium-turbidity raw water (≈50 NTU), 40, 60, 80, and 100 mg·L^{-1} of alum, all $\bar{G}$ values and 2.0 cm.min^{-1} of settling velocity.

However, a residual turbidity increase trend was observed with alum dosages of 60, 80, and 100 mg·L^{-1} as depicted in Figure 4. This indicates that the Al/particle ratios of 41, 54, and 68 mg Al^{3+}/g, respectively, may have contributed to the irreversible floc breakup. It is interesting to note that with increasing Al/particle ratio, the residual trend is notable even with lower $\bar{G}$ values. However, CoD values are considerably high for all fitted curves in Figure 4. It is assumed that the Al/particle ratio for these assays were not as high as those applied in the assays with low-turbidity raw water, resulting in less pronounced residual turbidity increase trends. This assumption supports the hypothesis that coagulant dosage plays a central role in the occurrence of this phenomenon.

High turbidity raw water assays

Figure 5 shows that with an alum dosage of 20 mg·L^{-1} (7 mg Al^{3+}/g ratio), the increase of residual turbidity was sharper in $\bar{G}$ values of 80 and 100 s^{-1}. The optimal range previously mentioned (14–27 mg Al^{3+}/g ratio) suggests that lower dosages may also lead to a residual turbidity increase. This may occur since the colloidal suspension may not be fully destabilized and fragile flocs could have been formed. CoD values were still high, suggesting that the increase in residual turbidity was not as pronounced as the ones observed with excessive dosage.

With alum dosages of 30, 40 and 60 mg·L^{-1}, the increase of residual turbidity was not significant, and CoD values were above 0.9 for all $\bar{G}$ values. The Al/particle ratios were 10, 14, and 20, respectively, suggesting that the previously mentioned range could be expanded from 10 to 27 mg Al^{3+}/g. However, with 80 mg·L^{-1} alum dosage (27 mg Al^{3+}/g ratio) the residual turbidity increase trend was observed (Figure 5) even though CoD values were still high (above 0.9 for all $\bar{G}$). This indicates that the trend in residual turbidity was again not so noticeable and the 27 mg Al^{3+}/g ratio may be slightly above the upper

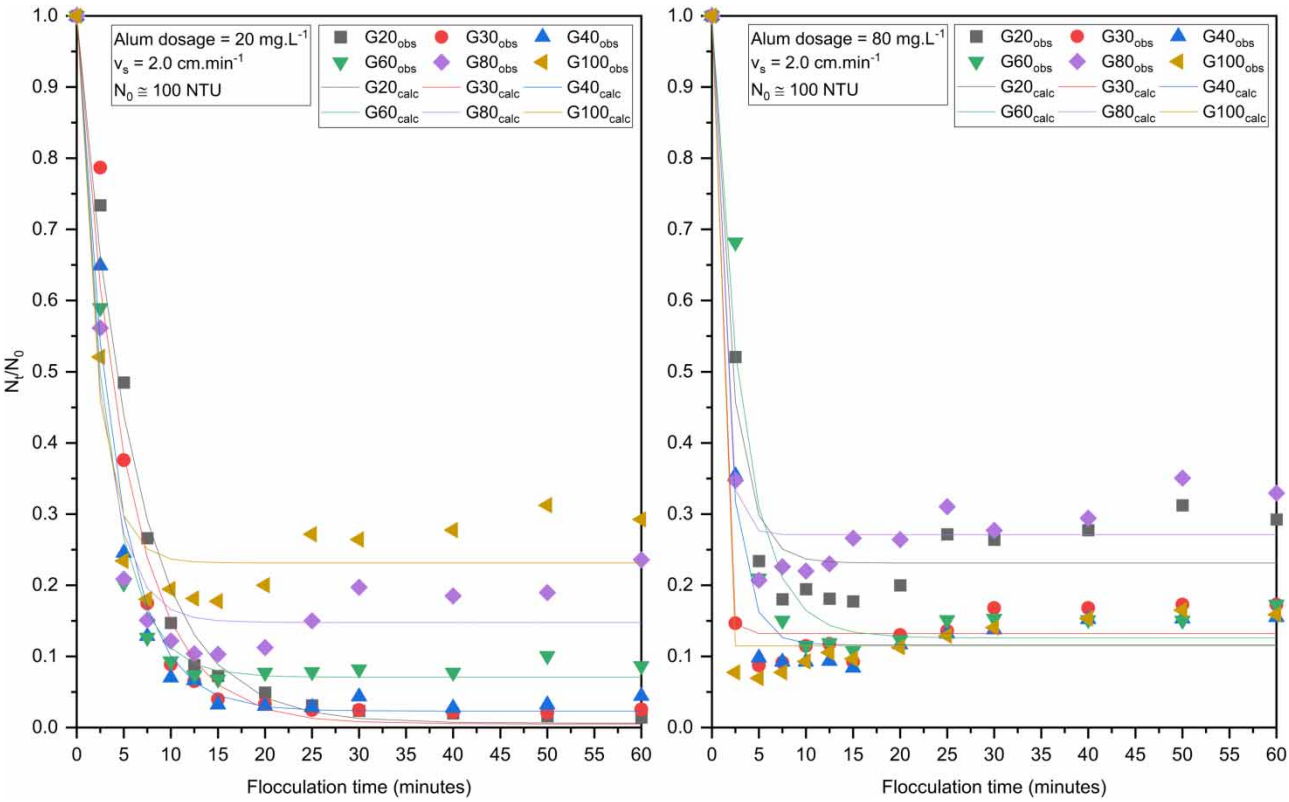

Figure 5 | Left: Model fitting to N_t/N_0 results with 20 mg·L^{-1} of alum. Right: Model fitting to N_t/N_0 results with 80 mg·L^{-1} of alum. All assays performed with high-turbidity raw water (≈100 NTU), all $\bar{G}$ values and 2.0 cm.min^{-1} of settling velocity.

limit in which this trend would not be observed. The residual turbidity trend was again observed with 100 mg·L^{-1} dosage of alum (34 mg Al^{3+}/g ratio), supporting the aforementioned range.

Results overview

Figure 6 shows the contour of minimum N_t/N_0 values and CoD values as a function of both $\bar{G}$ and Al/particle ratio. The lowest minimum N_t/N_0 values are in the left side of the contour (near the optimal range of 10–27 mg Al^{3+}/g ratio). Increasing $\bar{G}$ in this area does not directly reflect in higher minimum N_t/N_0 values. However, increasing Al/particle ratio produces higher minimum Nt/N_t values even with lower $\bar{G}$ values. Therefore, within the optimal Al/particle ratio range flocs were not easily broken even with increasing mixing intensity. With excessive dosages, however, there is a predominance of hydroxide precipitates, usually fragile and more susceptible to breakage. On the other hand, higher CoD values are in the lower left side of the contour, the same region as the lowest N_t/N_0 values. When Al/particle ratio increases, CoD values reduce, indicating poorer model fitting. Since experimental results indicated that higher Al/particle ratio led to the occurrence of the residual turbidity increase trend, this observation indicates that Argaman and Kaufman's original model may not be able to represent this phenomenon with high precision. As previously mentioned, it is assumed that the residual turbidity increase may be related to the irreversible floc breakup process, not considered in the original model formulation (Jarvis *et al.* 2005a; Marques & Ferreira Filho 2017).

Lastly, it is notable that the irreversible floc breakup was identified in all groups of assays (low, medium, and high turbidity raw water). Previous research has identified this phenomenon in particular water matrixes, such as the one used by Marques & Ferreira Filho (2017). In their work, the authors identified the irreversible floc breakup when studying flocculation kinetics of cyanobacteria contaminated water, a particular case of fragile flocs subjectable to breakup. All the assays described in this work were conducted with potable water spiked with kaolin particles, a rather common representation of surface water in lab scale. Therefore, it is possible that the irreversible floc breakup may occur regardless of the water matrix composition and should be accounted for in terms of flocculation process modelling.

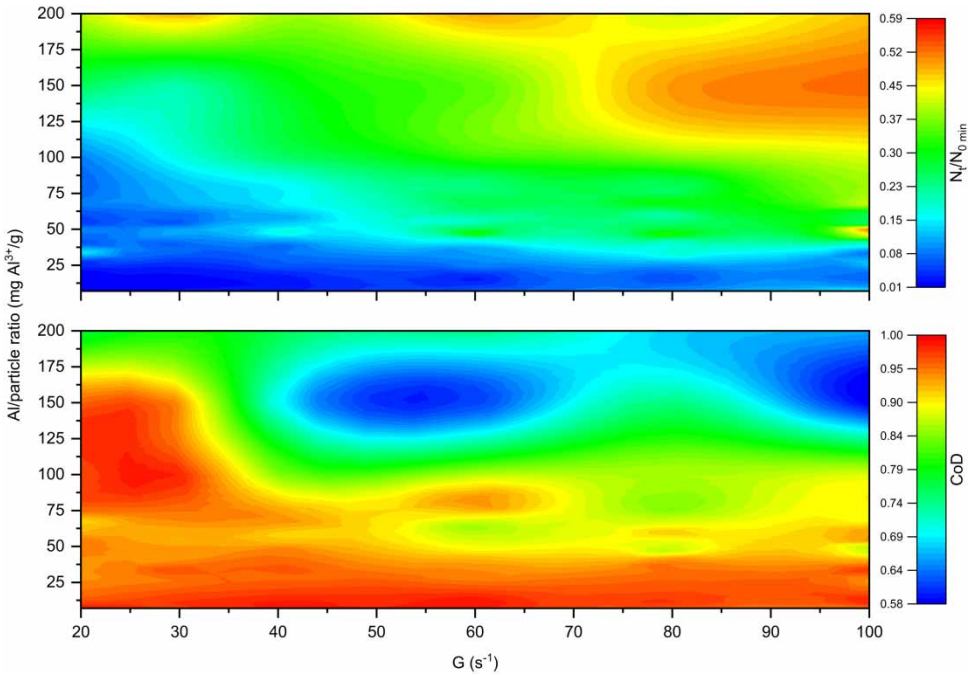

Figure 6 | Minimum N_t/N_0 and CoD values as function of $\bar{G}$ and Al/particle ratio.

K_A and K_B values and ANOVA results

All K_A and K_B values (also converted into pK_A and pK_B, respectively) are presented in the Supplementary Material. For the low-turbidity raw water assays, pK_B values were considerably higher (thus lower K_B) when Al/particle ratio was near 25 mg Al^{3+}/g and $\bar{G}$ was 20 and 30 s^{-1}. As previously mentioned, in those assays the equilibrium depicted by Argaman and Kaufman's model was not fully achieved, indicating a prevalence of the aggregation process with minimal breakup. Increasing $\bar{G}$ led to lower pK_B values and the equilibrium shown in Figure 2. With Al/particle ratios of 50 and 75 mg Al^{3+}/g, pK_B values were near 6 and 7 and with Al/particle ratios of 100, 150 and 200 mg Al^{3+}/g, pK_B values oscillated between 5 and 6. Considering previous observations, this could reflect a greater incidence of the irreversible breakup process, since it was previously identified in assays with excessive dosage. As for pK_A, with Al/particle ratios of 25, 50, and 75 mg Al^{3+}/g, its values were around 4. With higher Al/particle ratios, pK_A values oscillated between 3 and 4, reflecting the expected effect of increasing K_A with higher coagulant dosages.

As for the assays with medium-turbidity raw water, pK_B values were significantly higher when the Al/particle ratio was 14, 20, and 27 mg Al^{3+}/g, in agreement with the previously mentioned range. Increasing $\bar{G}$ value within these ratios led to lower pK_B values, indicating a greater incidence of the breakup process. Higher Al/particle led to a minimal reduction in pK_B values, thus suggesting that increasing coagulant dosage had a minor effect on the breakup process in these assays. As for pK_A, all values were near 4 within the entire Al/particle range, indicating that increasing coagulant dosage did not reflect significantly higher K_A values.

Within the assays with high turbidity raw water, it is notable that with the Al/particle ratio of 7 mg Al^{3+}/g the breakup process was evident, since pK_B values were not the highest. As previously mentioned, this Al/particle ratio may not be adequate to promote colloidal particle destabilization, thus producing fragile flocs. With Al/particle ratio of 10, 14, 20, and 27 mg Al^{3+}/g, the assays with $\bar{G}$ of 20 s^{-1} had the highest pK_B values. It is interesting to note that with 27 mg Al^{3+}/g the pK_B value in the assay with $\bar{G}$ value of 20 s^{-1} was still higher than with the other $\bar{G}$ values. However, it is considerably smaller than the pK_B values with 10, 14, and 20 Al/particle ratios. It is assumed that the 27 mg Al^{3+}/g ratio may be the upper limit in the optimal range. With the highest Al/particle ratio (34 mg Al^{3+}/g), slightly lower pK_B values were obtained, indicating a higher incidence of the breakup process without an apparent pattern with respect to $\bar{G}$. Considering the optimal range previously mentioned, it can be assumed that the 34 mg Al^{3+}/g ratio was excessive and therefore more likely to produce hydroxide flocs susceptible to irreversible breakup. However, since this ratio was not excessive as the ones applied in the low-turbidity raw water assays, the effect is less noticeable. Again, pK_A values remained near 4, except for the highest Al/particle ratio.

Table 1 | ANOVA results for pK_A and pK_B values

Source of Variation	SS	Df	MS	F	*P-value*	F_{crit}
pK_A						
Al/particle ratio	11.035	17	0.649	11.143	3.68×10^{-5}	1.744
$\bar{G}$	0.322	5	0.064	1.106	0.363	2.322
Error	4.951	85	0.058	–	–	–
Total	16.308	107	–	–	–	–
pK_B						
Al/particle ratio	513.560	17	30.209	6.721	7.86×10^{-10}	1.744
$\bar{G}$	159.247	5	31.849	7.086	1.40×10^{-05}	2.322
Error	382.075	85	4.495	–	–	–
Total	1054.881	107	–	–	–	–

A two-factor ANOVA without replication was conducted with pK_A and pK_B values, considering Al/particle and $\bar{G}$ as factors, presented in Table 1. Results indicated that a correlation may exist between pK_A values and the Al/particle ratio, which was expected since in Argaman and Kaufman's model K_A is proportional to floc volume and, therefore, to coagulant dosage. ANOVA also indicated that a correlation between pK_A and $\bar{G}$ was not clear. Considering that K_A is proportional to K_s and K_P (Equation (2)), it is assumed that all $\bar{G}$ values promoted sufficient particle collision. Therefore, coagulant dosage was the variable that influenced K_A the most (AWWA 2011; Crittenden *et al.* 2012; Bratby 2016).

ANOVA also indicated that there may be a correlation between pK_B and Al/particle as well as between pK_B and $\bar{G}$. Equation (3) shows that the K_B value is directly influenced by K_p squared, thus it is more sensitive to mixing conditions. However, it is interesting to note a possible correlation between pK_B and Al/particle ratio. Coagulant dosage is usually mentioned when discussing K_A and the aggregation process. However, it is reasonable to expect that coagulant dosage may also influence the breakup process, since it is the metal ion and its hydrolysis products that allow floc formation. Argaman and Kaufman's model is constructed in such a way that K_B is influenced by coagulant dosage, as previously mentioned when discussing Equation (3) (K_B is related to floc volume and, therefore, to coagulant dosage). However, the model is not able to represent the residual turbidity increase trend identified in this work, attributed to the irreversible floc breakup. A modification of the original model, including a specific term for this process may result in better fitting to experimental results in these conditions (Marques & Ferreira Filho 2017).

CONCLUSIONS

In this work, flocculation kinetics of different turbidity raw water was studied using Argaman and Kaufman's original model. Most of the experimental results were satisfactorily described by the model with high CoD values. However, in certain conditions a residual turbidity increase trend was observed, not adequately described by the model. This trend was attributed to the irreversible floc breakup process and was more pronounced when coagulant dosage resulted in Al/particle ratios outside an optimal range of 10 and 27 mg Al^{3+}/g. The $\bar{G}$ value was also an important factor, since increasing mixing intensified the observed trend. Since it was identified in all groups of assays, it is possible that the irreversible floc breakup may occur regardless of the water matrix composition and should be accounted for in terms of flocculation process modeling. Model coefficients K_A and K_B values were calculated, and the results reflected experimental observations. It is recommended to analyze this works results with different flocculation models for better representation of the irreversible floc breakup process. One promising approach is applying the modified version of Argaman and Kaufman's model presented by Marques & Ferreira Filho (2017). This is going to be the topic of future research.

DATA AVAILABILITY STATEMENT

All relevant data are included in the paper or its Supplementary Information.

REFERENCES

Argaman, Y. & Kaufman, W. J. 1970 Turbulence and flocculation. *J. Sanit. Eng. Div.* **96**, 223–241.

AWWA 2011 *Water Quality and Treatment: A Handbook on Drinking Water*, 6th edn. McGraw Hill, New York, USA.

Brandt, S. 2014 *Data Analysis – Statistical and Computational Methods for Scientists and Engineers*, 4th edn. Springer International Publishing Switzerland, New York, USA.

Bratby, J. R. 1981 Interpreting laboratory results for the design of rapid mixing and flocculation systems. *J. AWWA* **73**, 318–325.

Bratby, J. R. 2016 *Coagulation and Flocculation in Water and Wastewater Treatment*, 3rd edn. IWA Publishing, London, UK.

Chapra, S. C. & Canale, R. P. 2015 *Numerical Methods for Engineers*, 7th edn. McGraw-Hill Education, New York, USA.

Crittenden, J. C., Trussell, R. R., Hand, D. W., Howe, K. J. & Tchobanoglous, G. 2012 *MWH's Water Treatment: Principles and Design*, 3rd edn. John Wiley & Sons Inc., Hoboken, USA.

Di Bernardo, L., Botari, A. & Sabogal-Paz, L. P. 2005 Uso de modelação matemática para projeto de câmaras mecanizadas de floculação em série em estações de tratamento de água. *Eng. Sanit. e Ambient.* **10**, 82–90.

Di Bernardo, L., Dantas, A. D. B. & Voltan, P. E. N. 2017 *Métodos e Técnicas de Tratamento de Água*, 3rd edn. LDiBe Editora, São Carlos, Brazil.

Dobre, T. G. & Sanchez Marcano, J. G. 2007 *Chemical Engineering: Modelling, Simulation and Similitude*, 1st edn. WILEY-VCH Verlag GmbH & Co., Weinheim, Germany.

Ferreira Filho, S. S. 2017 *Tratamento de Água: Concepção, projeto e operação de estações de tratamento*, 1st edn. Elsevier Editora Ltda., Rio de Janeiro, Brazil.

Ferreira Filho, S. S., Hespanhol, I. & Moreira, H. A. 2000 Flocculation Kinetics of Colloidal Suspensions: Effects of Metallic Coagulant Dosage and Primary Particle Concentration on the Breakup and Aggregation Constants. In: *Chemical Water and Wastewater Treatment VI: Proceedings of the 9th Gothenburg Symposium*. Springer Berlin Heidelberg, New York, pp. 101–109.

Haarhoff, J. & Joubert, H. 1997 Determination of aggregation and breakup constants during flocculation. *Water Sci. Technol.* **36**, 33–40.

Jarvis, P., Jefferson, B. & Parsons, S. 2004 The duplicity of floc strength. *Water Sci. Technol.* **50**, 63–70.

Jarvis, P., Jefferson, B., Gregory, J. & Parsons, S. A. 2005a A review of floc strength and breakage. *Water Res.* **39**, 3121–3137.

Jarvis, P., Jefferson, B. & Parsons, S. A. 2005b Breakage, regrowth, and fractal nature of natural organic matter flocs. *Environ. Sci. Technol.* **39**, 2307–2314.

Levenspiel, O. 1999 *Chemical Reaction Engineering*, 3rd edn. John Wiley & Sons, Inc., New York, USA.

Marques, R. d. O. & Ferreira Filho, S. S. 2017 Flocculation kinetics of low-turbidity raw water and the irreversible floc breakup process. *Environ. Technol.* **38**, 901–910.

Moruzzi, R. B. & de Oliveira, S. C. 2013 Mathematical modeling and analysis of the flocculation process in chambers in series. *Bioprocess Biosyst. Eng.* **36**, 357–363.

Rice, E. W., Baird, R. B., Eaton, A. D. & Clesceri, L. 2012 *Standard Methods for the Examination of Water and Wastewater*, 22nd edn. American Publich Health Association, American Water Works Association, Water Environment Federation, Washington, USA.

Tassinari, B., Conaghan, S., Freeland, B. & Marison, I. W. 2015 Application of turbidity meters for the quantitative analysis of flocculation in a Jar test apparatus. *J. Environ. Eng.* **141**, 1–8.

Thomas, D. N., Judd, S. J. & Fawcett, N. 1999 Flocculation modelling: a review. *Water Res.* **33**, 1579–1592.

Von Sperling, M., Verbyla, M. E. & Oliveira, S. M. A. C. 2020 *Assessment of Treatment Plant Performance and Water Quality Data – A Guide for Students, Researchers and Practitioners*, 1st edn. IWA Publishing, London, UK.

Watanabe, Y. 2017 Flocculation and me. *Water Res.* **114**, 88–103.

Winston, W. L. 2016 *Microsoft Excel 2016 - Data Analysis and Business Modeling*, 1st edn. Microsoft Press, Redmond, USA.

First received 9 August 2021; accepted in revised form 28 December 2021. Available online 19 January 2022